

Exfoliated–Restacked Phase of WS₂Hui-Lien Tsai,[†] Joy Heising,[†] Jon L. Schindler,[‡]
Carl R. Kannewurf,[‡] and Mercuri G. Kanatzidis*[†]Department of Chemistry and
Center for Fundamental Materials Research
Michigan State University,
East Lansing, Michigan 48824Department of Electrical Engineering and
Computer Science
Northwestern University, Evanston, Illinois 60208

Received November 8, 1996

Revised Manuscript Received February 24, 1997

The best known forms of the sulfides of Mo and W are 2H-MoS₂ and 2H-WS₂. Much less is known about the so-called 1T forms of these compounds, which are analogous to 1T-TiS₂, where the metal center is in an octahedral coordination environment. The 2H-MoS₂ and 2H-WS₂ are distinguished among the metal dichalcogenides for not intercalating organic molecules such as pyridine, ammonia, etc. This intercalative inertness originates from the prismatic coordination environment of Mo and W centers (d² configuration) which results in a fully occupied valence band composed of d_{z²} levels which stabilizes the system and causes a large energy gap. To insert guest molecules in MoS₂ or WS₂, one must proceed indirectly via the hydrolysis of LiMoS₂, which releases single layers in solution.¹ The LiMoS₂ is typically achieved by reaction of MoS₂ with *n*-butyllithium in hexane.² Reprecipitation of the layers in the presence of small molecules results in intercalation compounds.³ We have exploited this property to produce novel polymer/MoS₂ nanocomposites.⁴ WS₂ is harder to reduce than MoS₂ and intercalation is possible only with highly reducing agents such as alkali and alkaline-earth metals^{5,6a} or with *n*-butyllithium in hexane.⁷ In our hands reduction of WS₂ with *n*-butyllithium does not lead to completely exfoliatable material, in contrast to MoS₂, which works very well. In this communication we report a new convenient method to

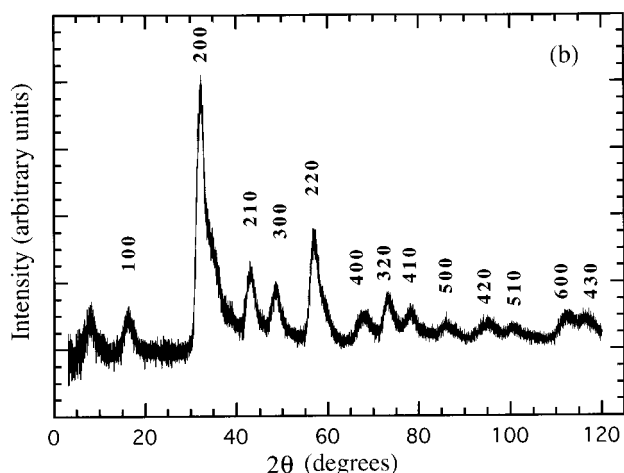
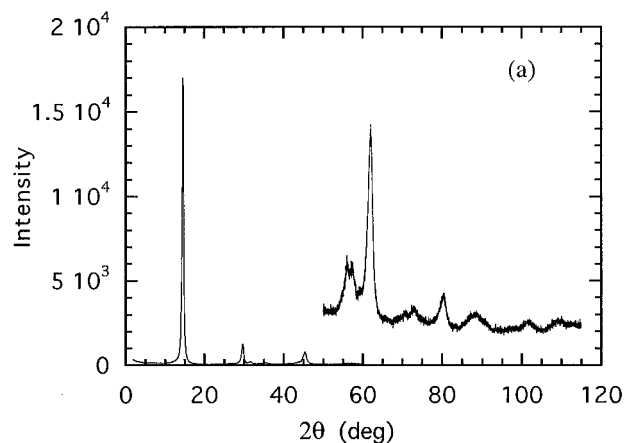
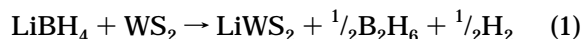


Figure 1. Typical X-ray diffraction patterns of an anhydrous exfoliated–restacked WS₂ film (a) in reflection (X-ray beam at grazing angle) and (b) in transmission geometry (X-ray beam perpendicular to film).

prepare large quantities of LiWS₂, using a new lithium intercalation technique involving LiBH₄, and the subsequent conversion of the lithiated material to 1T'-WS₂⁸ using an exfoliation–restacking procedure. We also report the physicochemical, X-ray crystallographic, and for the first time electron crystallographic and electrical transport characterization of 1T'-WS₂.

A mixture of LiBH₄ and WS₂ in the molar ratio 2.5:1 was loaded into a 5 mL alumina tube, and this alumina tube was loaded into a 50 cm long, 13 mm width Pyrex tube with a gas outlet in a nitrogen atmosphere glovebox. The mixture was heated to 350 °C over 12 h for 3 days and cooled to 50 °C over 12 h. The reaction involves the Li insertion in WS₂, and oxidative decomposition of LiBH₄ according to eq 1. This reaction is



convenient because the byproducts are all gases, which escape to leave only the product thus eliminating the

(8) (a) The term 1T- corresponds to a crystalline phase with three-dimensional order. Because of the isostructural relationship of the single layers of restacked WS₂ and those of the 1T- form, we choose to use the term 1T' for the material dealt with in this communication. Given that the single layers of MoS₂ and WS₂ encapsulate cations, the exfoliated–restacked or 1T'-WS₂ may actually be a lithium or hydrogen bronze depending on the method of preparation. Therefore, the 1T'-WS₂ designation refers only to the product of the exfoliation/restacking procedure, and not necessarily to a bona fide molecular formula. (b) See: Heising, J.; Kanatzidis, M. G., to be published.

[†] Michigan State University.

[‡] Northwestern University.

(1) (a) Joensen, P.; Frindt, R. F.; Morrison, S. R. *Mater. Res. Bull.* **1986**, *21*, 457–461. (b) Divigalpitiya, W. M. R.; Frindt, R. F.; Morrison, S. R. *Thin Solid Films* **1990**, *186*, 177–192. (c) Divigalpitiya, W. M. R.; Frindt, R. F.; Morrison, S. R. *Appl. Surf. Sci.* **1991**, *48/49*, 572–575.

(2) Murphy, D. W.; DiSalvo, F. J.; Hull, G. W.; Waszczak, J. V. *Inorg. Chem.* **1976**, *15*, 17–21.

(3) (a) Gee, M. A.; Frindt, R. F.; Joensen, P.; Morrison, S. R. *Mater. Res. Bull.* **1986**, *21*, 543–549. (b) Divigalpitiya, W. M. R.; Frindt, R. F.; Morrison, S. R. *Science* **1989**, *246*, 369–371. (c) Divigalpitiya, W. M. R.; Frindt, R. F.; Morrison, S. R. *J. Mater. Res.* **1991**, *6*, 1103–1107. (d) Tagaya, H.; Hashimoto, T.; Karasu, M.; Izumi, T.; Chiba, K. *Chem. Lett.* **1991**, *12*, 2113–2116.

(4) (a) Kanatzidis, M. G.; Bissessur, R.; DeGroot, D. C.; Schindler, J. L.; Kannewurf, C. R. *Chem. Mater.* **1993**, *5*, 595–596. (b) Bissessur, R.; Kanatzidis, M. G.; Schindler, J. L.; Kannewurf, C. R. *J. Chem. Soc., Chem. Commun.* **1993**, 1582–1585. (c) Bissessur, R.; Schindler, J. L.; Kannewurf, C. R.; Kanatzidis, M. G. *Mol. Cryst. Liq. Cryst.* **1993**, *245*, 249–254. (d) Wang, L.; Schindler, J. L.; Thomas, J. A.; Kannewurf, C. R.; Kanatzidis, M. G. *Chem. Mater.* **1995**, *7*, 1753–1755.

(5) (a) Rudorff, W. *Chimia* **1965**, *19*, 489–499. (b) Bayer, E.; Rudorff, W. *Z. Naturforsch.* **1972**, *27b*, 1336–1339. (c) Schöllhorn, R.; Bethel, U.; Paulus, W. *Rev. Chim. Miner.* **1984**, *21*, 545–555.

(6) (a) Miremedi, B. K.; Morrison, S. R. *J. Appl. Phys.* **1988**, *63*, 4970–4974. (b) Miremedi, B. K.; Morrison, S. R. *J. Appl. Phys.* **1990**, *67*, 1515–1520.

(7) Yang, D.; Frindt, R. F. *J. Phys. Chem. Solids* **1996**, *57*, 1113–1116.

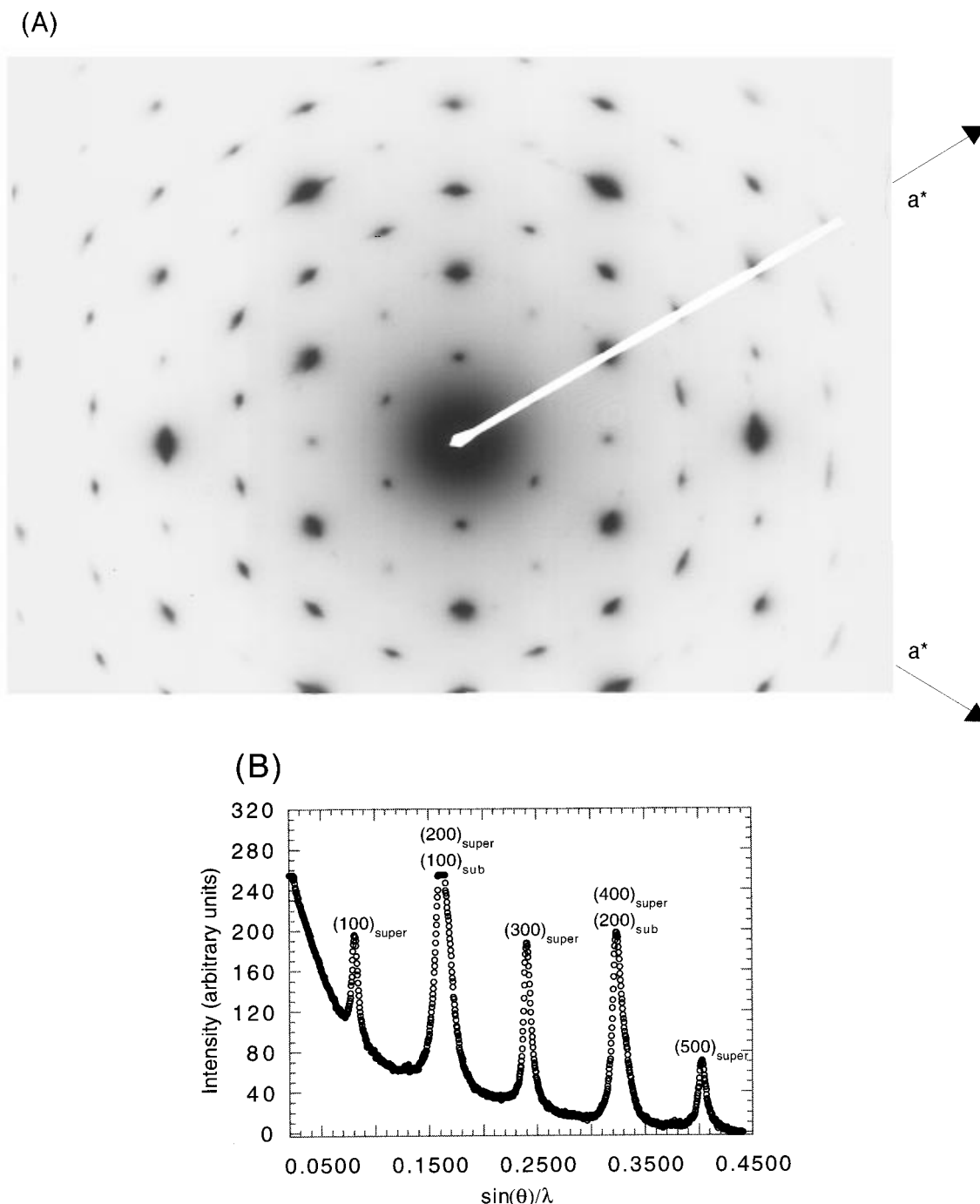


Figure 2. (A) Selected area electron diffraction pattern with the beam perpendicular to the layers ([001] direction) from restacked WS_2 showing the $2a \times 2a$ superlattice. (B) Densitometric intensity profile along the a^* axis of the electron diffraction pattern showing the $(h00)_{\text{superlattice}}$ family of reflections. The peaks are labeled with their $2a \times 2a$ superlattice indices. The rising background under the diffraction pattern is due to diffuse scattering of inelastically scattered electrons.

need for solvents and the isolation procedure. This reaction can be easily scaled up and 10–15 g batches of LiWS_2 have been prepared readily.

The resulting LiWS_2 powder exfoliates very well in water into single layers with the evolution of hydrogen gas. The solid product can be obtained by centrifuging the single-layer suspension and decanting the supernatant aqueous phase. As has been explained before, this process results in $1\text{T}'\text{-WS}_2$ in which the W metal is octahedrally coordinated.^{1,3} Well-ordered hydrated WS_2 films can be prepared by spreading the single-layer suspension on Saran film or other substrates. Dehydrated product can be obtained by washing with HCl

and pumping in vacuo for 12 h. X-ray diffraction diagrams of the films were obtained in both reflection and transmission⁹ modes (see Figure 1). The reflection diffraction patterns show that the hydrated WS_2 phase has an interlayer spacing of 11.30 Å, while the anhydrous phase has 6.25 Å.

Although it is well established that the metal coordination environment differs in the two forms (trigonal prismatic vs octahedral), a particularly important ques-

(9) That only $(00l)$ and $(hk0)$ reflections are observed in the reflection and transmission X-ray diffraction geometry respectively indicates that the films consist of well stacked WS_2 slabs of turbostratic character. Randomly oriented powders do not show (hkl) reflections.

Table 1. Indices (*hk*0), Angles, and Experimental *d* Spacings Determined from X-ray Transmission Diffraction Experiments on 1T'-WS₂ Oriented Films^a

<i>hk</i> 0	2θ/deg	<i>d</i> spacing/Å
100	15.92	5.567
200	32.16	2.783
210	42.86	2.110
300	48.40	1.881
220	56.89	1.619
400	67.77	1.383
320	73.13	1.294
410	78.29	1.221
500	86.04	1.130
420	94.90	1.046
510	100.81	1.000
600	112.43	0.928
430	116.12	0.908

^a The data are indexed to a 6.32 Å × 6.32 Å lattice.

tion is that of the in-plane structural arrangement of the metal and sulfur atoms. In the absence of any superstructure the ideal arrangement is the same as that of 1T-TiS₂. However, it is now clear that in these materials a longer range periodicity exists.^{7,10} Therefore, in-plane structural information in restacked WS₂ was sought with X-ray diffraction in transmission geometry. Only (*hk*0) reflections are observed in the pattern (see Figure 1b) which can be indexed to a 2*a* × 2*a* superlattice of trigonal symmetry, in agreement with the recent results on suspended single layers of WS₂.⁷ The indices of the (*hk*0) reflections, 2θ angles, and *d* values are listed in Table 1. Complementary to the X-ray diffraction results, electron diffraction, performed on a JEOL 100CX transmission electron microscope (TEM) operating at 120 kV, from thin microcrystals of freshly exfoliated WS₂ with the beam parallel to the *c* axis confirm the presence of superlattice. The 2*a* × 2*a* supercell is clearly visible in Figure 2A. Figure 2B shows a densitometric scan along the *a** axis and the intensity profile of the (*h*00) set of reflections. The weaker set of superlattice reflections lie half-way between the strong sublattice reflections with *a**_{super} = 0.5*a**_{sub}.

The presence of the superlattice peaks in both the X-ray and the electron diffraction patterns suggests a significant displacement of the W atoms (and possibly the S atoms) from their ideal positions in the hexagonal P-3m1 arrangement of 1T-TiS₂ structure type. It is important to note that the hexagonal symmetry of the diffraction pattern suggests a distortion in which the structure preserves the crystallographic 3-fold axis. The 2*a* × 2*a* superlattice is in disagreement with the √3*a* × √3*a* superlattice predicted for isostructural layered systems with a *d*² electron configuration (e.g., 1T-MS₂ with *d*²).¹¹ There is always, of course, the possibility that the material we are observing is a merohedral crystallographic twin (actually triplet) of a 2 × 1 superstructure.¹² A structural analysis study of the observed 2*a* × 2*a* superlattice is currently underway.

(10) Yang, D.; Jiménez Sandoval, S.; Divigalpitiya, W. M. R.; Irwin, J. C.; Frindt, R. F. *Phys. Rev. B* **1991**, *43*, 12053–12056.

(11) Rovira, C.; Whangbo, M.-H. *Inorg. Chem.* **1993**, *32*, 4094–4097.

(12) (a) AFM studies on restacked MoS₂ have shown that at least the top layer exhibits a 2 × 1 superstructure. If every layer in the restacked sample has a 2 × 1 superstructure then the observed diffraction data could be interpreted in terms of a twinned model in which individual layers are rotated exactly 120° with respect to one another. (b) Qin, X. R.; Yang, D.; Frindt, R. F.; Irwin, J. C. *Ultramicroscopy* **1992**, *42–44*, 630–636.

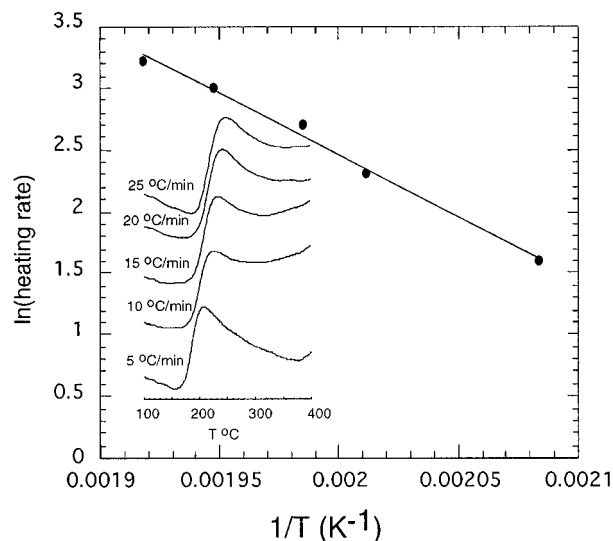


Figure 3. Kinetic Arrhenius plot for the conversion of exfoliated–restacked WS₂ to the 2H form. Inset: DSC plots as a function of heating rate.

Restacked WS₂ undergoes an irreversible, exothermic phase transition at 207 °C (heating rate 5 K/min) to 2H-WS₂, which indicates that it is metastable.¹³ Restacked MoS₂ is also metastable and converts to the 2H-MoS₂ at ~92 °C.¹⁴ The kinetics of this transformation were studied by monitoring the peak position of the transformation temperature as a function of heating rate.¹⁵ The position of exothermic peaks shift to higher temperatures with increasing heating rates (see Figure 3A). Fitting the data to the Arrhenius type equation (eq 2) leads to the activation energy of the transformation:

$$\ln(b) = -E_a/RT_{\max} + A \quad (2)$$

where *b* is the heating rate in K/min, *E_a* is the activation energy in J/mol, *R* is the molar gas constant (8.3144 J mol⁻¹ K⁻¹), *T_{max}* is the temperature at which the maximum of the exothermic peak occurs and *A* is a constant. Figure 3B shows the fit of the data to eq 2 and from the slope of the line corresponds to an activation energy of 82.4 kJ/mol. This value is substantially higher than that observed for MoS₂¹⁶ and is consistent with the higher temperature of the phase transition for WS₂.

The electrical conductivity of exfoliated–restacked WS₂ was measured by four-probe electrical conductivity measurements of pressed pellet samples in the temperature range 7–300 K (see Figure 4A). The material is highly conductive at room temperature, reaching values of ~7 S/cm, an order of magnitude higher than the conductivity of the Mo analogue measured under identical conditions. As a function of temperature the data exhibit a very weak dependence and the material remains conductive even at 5 K (see Figure 4). Since the accurate in-plane structure of this material is not yet established, it is difficult to account for the observed

(13) Examined with differential scanning calorimetry (DSC). If indeed the restacked materials are bronzes, the exothermic conversion must also involve a redox step.^{8b}

(14) Wypych, F.; Schöllhorn, R. *J. Chem. Soc., Chem. Commun.* **1992**, 1386–1388.

(15) *Annual Book of ASTM Standards* **1979**, E-698, 601–608.

(16) (a) Bissessur, R.; Kanatzidis, M. G., unpublished work. (b) Bissessur, R. Ph.D. Thesis, Michigan State University, 1994.

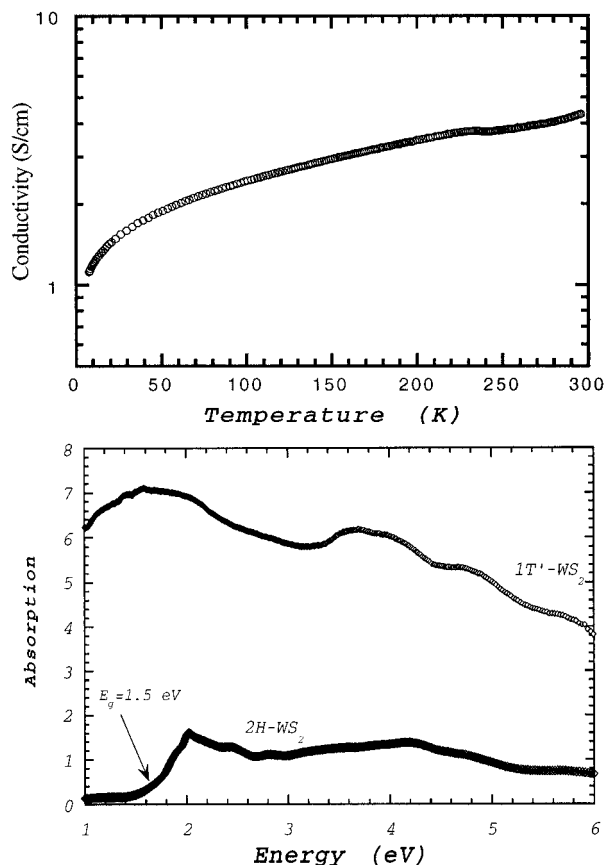


Figure 4. (A) Four-probe variable-temperature electrical conductivity data for pressed sample of exfoliated–restacked WS_2 . (B) Electronic absorption data for semiconducting 2H-WS_2 and the metallic $1\text{T}'$ -analogue.

conductivity on the basis of an electronic band picture. As we have discussed earlier, however, the ideal structure of 1T-MoS_2 (undistorted) does lead to metallic bands.^{4b} We believe that the restacked WS_2 and MoS_2 are isostructural and thus have similar electronic properties. The relatively high conductivity of the

restacked WS_2 suggests that the structural $2a \times 2a$ distortion present in the layers does not remove completely the energy states from the Fermi level. Magnetic susceptibility measurements show Pauli paramagnetism and suggest a metallic nature to the material. What remains to be determined is the how exact nature of the structural distortion, which leads to the trigonal $2a \times 2a$ superstructure, affects these bands. The application of temperature ($>208^\circ\text{C}$) or high pressure leads irreversibly to a semiconductor with conductivity of $<10^{-5}$ S/cm, consistent with conversion to 2H-WS_2 . Absorption spectroscopy highlights the dramatic differences in electronic structure between the 2H- and restacked forms of WS_2 . The latter material strongly absorbs at all frequencies consistent with no energy gap at the Fermi level, in sharp contrast to the 2H- form, which exhibits an overall lower absorptivity and a gap at ~ 1.5 eV (Figure 4B).

In summary, the exfoliated-restacked WS_2 (or $1\text{T}'\text{-WS}_2$) phase exhibits a $2a \times 2a$ superstructure at room temperature and it is metastable with respect to 2H-WS_2 , converting at 207°C . However, it is considerably less metastable than 1T-MoS_2 which converts at 91°C . The new lithiation method of 2H-WS_2 , using LiBH_4 , is amenable to large scale reactions and gives high yields of exfoliated WS_2 material, thus opening the way to a new class of intercalative polymer/ WS_2 nanocomposites and other intercalation compounds.^{17,18}

Acknowledgment. Financial support from the National Science Foundation (DMR-93-06385) is gratefully acknowledged. This work made use of the TEM facilities of the Center for Electron Optics at Michigan State University. At Northwestern University this work made use of Central Facilities supported by the NSF through the Materials Research Center.

CM960579T

(17) Tsai, H.-L.; Wang, L.; Heising, J.; Kanatzidis, M. G., to be submitted for publication.

(18) The details and scope of the LiBH_4 method will be reported elsewhere. Wang, L.; Kanatzidis, M. G., to be published.